NOAA Technical Report ERL 448–WPL 64

# Relationship of Height Gradients of Passive Atmospheric Properties to Their Variances: Applications to the Ground-Based Sensing of Profiles

E.E. Gossard

August 1992

**U.S. DEPARTMENT OF COMMERCE**
National Oceanic and Atmospheric Administration
Environmental Research Laboratories

NOAA Technical Report ERL 448–WPL 64

# Relationship of Height Gradients of Passive Atmospheric Properties to Their Variances: Applications to the Ground-Based Sensing of Profiles

E.E. Gossard
Cooperative Institute for Research in
Environmental Sciences (CIRES)

Wave Propagation Laboratory
Boulder, Colorado

August 1992



**U.S. Department of Commerce**
Barbara Hackman Franklin, Secretary

National Oceanic and Atmospheric Administration
John A. Knauss, Under Secretary for Oceans and Atmosphere/Administrator

Environmental Research Laboratories
Boulder, Colorado
Joseph O. Fletcher, Director

## NOTICE

Mention of a commercial company or product does not constitute an endorsement by NOAA/Environmental Research Laboratories. Use of information from this publication concerning proprietary products or the tests of such products for publicity or advertising purposes is not authorized.

For sale by the National Technical Information Service, 5285 Port Royal Road
Springfield, VA 22061

# CONTENTS

# Relationship of Height Gradients of Passive Atmospheric Properties to Their Variances: Applications to the Ground-Based Sensing of Profiles

**Earl E. Gossard**

**ABSTRACT.** Ways of relating height profiles of mean atmospheric properties to their variances are compared. Assuming a horizontally homogeneous, time-stationary medium, all methods assert the proportionality of the variance of a property $\chi$ to the variance of the turbulent velocity in the medium, to the square of the height gradient of the mean, and to the inverse Väisälä-Brunt frequency squared. This paper examines the dependence of the proportionality factor on the Richardson number. Finally, the various options for retrieving humidity profiles and refractive index profiles from radar wind profiler data are discussed, and reasons are given why a system that makes use of the acoustic backscatter as well as the radar backscatter is attractive.

## 1. INTRODUCTION

Because radar and acoustic sounders sense backscatter from the turbulent perturbations of refractive index, it is necessary to relate the intensity of the perturbations (say, their variance or their structure parameter) to the gradient of the mean, if profiles of the mean properties are to be retrieved. Derivations of the relationship between height profiles of mean atmospheric properties and their variances have usually started from the energy equation. Then, with assumptions about the spectral forms of the perturbations of the property and the turbulent velocity in the medium, it is found that

$$C_\chi^{\,2} = C_1 \frac{C_V^{\,2}}{\omega_B^{\,2}} \left( \frac{\partial \chi_0}{\partial z} \right)^2 . \qquad (1)$$

Assuming homogeneous, steady, isotropic turbulence, we will show that

$$C_1 = \frac{B_\chi}{B} \left( \frac{\mathrm{Ri}}{\mathrm{Pr} - \mathrm{Ri}} \right) . \qquad (2)$$

In Eq. (1), $\chi$ is some property (such as humidity or potential refractive index); $\chi_0(z)$ is the height distribution of its mean, or unperturbed, value, and $C_\chi^{\,2}$ is its structure parameter. Ri and Pr are the Richardson number and turbulent Prandtl number, respectively; $C_V^{\,2}$ is the velocity structure parameter of the medium; $\omega_B$ is the Väisälä-Brunt frequency; $B_\chi$ and $B$

are Kolmogoroff constants. Gossard and Sengupta (1988) presented evidence that $C_1$ is on the order of unity over a substantial range of stability. It is the purpose of the current paper to generalize this result and clarify the behavior of the factor $C_1$.

## 2. VARIANCE BALANCE EQUATIONS FOR DISSIPATION AND GENERATION IN EQUILIBRIUM

We consider here the variance budgets for classical turbulence (see, e.g., Tatarskii, 1971). Some relatively simple relationships between variance and gradient, under atmospheric conditions of static stability and shear, can be derived if it is assumed that the inertial subrange exists over the turbulence scales of interest. For example, in homogeneous isotropic turbulence, the one-dimensional velocity and temperature spectra are given, respectively, by (see any standard turbulence text, e.g., Tatarskii, 1971)

$$S_V(k) = A\,\varepsilon^{2/3}\,k^{-5/3} = \frac{A}{B}\,C_V^{\,2}\,k^{-5/3}\ , \tag{3}$$

and

$$S_\theta(k) = A_\theta\,\varepsilon^{-1/3}\,\varepsilon_\theta\,k^{-5/3} = \frac{A_\theta}{B_\theta}\,C_\theta^{\,2}\,k^{-5/3}\ . \tag{4}$$

Here, $k$ is the wavenumber in the turbulence spectrum; $\varepsilon$ is the turbulent dissipation rate of kinetic energy; $\varepsilon_\theta$ is the dissipation of half-variance of temperature; $A$ is a universal constant equal to about 0.5 for the wind component parallel to the flow and to about 0.67 for components perpendicular to it; $B = 4A$ ; and $C_V^{\,2}$ is the velocity structure parameter. $A_\theta$ and $B_\theta$ are universal constants equal to 0.8 and 3.2, respectively, and $C_\theta^{\,2}$ is the temperature structure parameter. The energy balance equation and the corresponding temperature half-variance balance equation for steady-state conditions can be written, respectively (e.g., Lumley and Panofsky, 1964), as

$$\varepsilon = -\langle wu\rangle\,\frac{\partial u_0}{\partial z}\,(1 - R_f)\ , \tag{5}$$

$$\varepsilon_\theta = -\langle \theta w\rangle\,\frac{\partial \theta_0}{\partial z}\ , \tag{6}$$

where angle brackets denote average, and where pressure covariance terms and divergence of flux of variance have been neglected. In (5) and (6), $u$ and $w$ are the perturbations of

horizontal and vertical velocity, respectively, and $\theta$ is the potential temperature perturbation; $\partial u_0/\partial z$ and $\partial \theta_0/\partial z$ are the gradients with height of the unperturbed horizontal velocity and unperturbed potential temperature. The flux Richardson number

$$R_f = \frac{[(g/\theta_0)\langle w\theta\rangle}{\langle uw\rangle(\partial u_0/\partial z)} = \frac{K_\theta}{K_V}\,\mathrm{Ri}\ .$$

Ri is the gradient Richardson number given by

$$\mathrm{Ri} = \omega_B{}^2\left(\frac{\partial u_0}{\partial z}\right)^{-2}\ , \tag{7}$$

where $\omega_B = [(g/\theta_0)(d\theta_0/dz)]^{1/2}$ is the Väisälä-Brunt frequency, and $g$ is the acceleration of gravity. The eddy coefficients $K_\theta$ and $K_V$ are defined as $K_\theta = -\langle w\theta\rangle/(\partial\theta_0/\partial z)$ and $K_V = -\langle wu\rangle/(\partial u_0/\partial z)$, and therefore (5) can be written [using (3)]

$$K_V = \frac{\varepsilon}{\left(\frac{\partial u_0}{\partial z}\right)^2(1-R_f)} \equiv \frac{(C_V{}^2/B)^{3/2}}{\left(\frac{\partial u_0}{\partial z}\right)^2}(1-R_f)^{-1}\ . \tag{8}$$

Furthermore, turbulence similarity considerations lead to the conclusion that the temperature structure parameter $C_\theta{}^2$ is related to the rate of dissipation of temperature half-variance $\varepsilon_\theta$ by (Corrsin, 1951)

$$C_\theta{}^2 = B_\theta\,\varepsilon^{-1/3}\,\varepsilon_\theta\ . \tag{9}$$

Noting that $B\,\varepsilon^{2/3} = C_V{}^2$ [i.e., see (3)], we obtain

$$C_\theta{}^2 = B_\theta\left(\frac{C_V{}^2}{B}\right)^{-1/2}\left(\frac{K_\theta}{K_V}\right)K_V\left(\frac{\partial\theta_0}{\partial z}\right)^2\ . \tag{10}$$

So, after (8) is used to eliminate $K_V$, these equations and definitions lead to the fundamental relationship between the velocity and temperature structure parameters and the velocity and temperature gradients; i.e.,

$$C_\theta^2 \left( \frac{\partial \theta_0}{\partial z} \right)^{-2} = \frac{B_\theta}{B} \left( \frac{K_V}{K_\theta} - \mathrm{Ri} \right)^{-1} \left[ C_V^2 \left( \frac{\partial V_M}{\partial z} \right)^{-2} \right], \tag{11}$$

where $V_M$ is defined by

$$\left( \frac{\partial V_M}{\partial z} \right)^2 = \left( \frac{\partial u_0}{\partial z} \right)^2 + \left( \frac{\partial v_0}{\partial z} \right)^2 .$$

$K_V/K_\theta$ is a ratio often called the turbulent Prandtl number, Pr. Eliminating the shear by using (7), we readily see that

$$C_\theta^2 \left( \frac{g}{\theta_0} \frac{\partial \theta_0}{\partial z} \right) = \frac{B_\theta}{B} \left( \frac{\mathrm{Ri}}{\mathrm{Pr} - \mathrm{Ri}} \right) C_V^2 \left( \frac{\partial \theta_0}{\partial z} \right)^2 . \tag{12}$$

This expression has been widely used (e.g., Van Zandt et al., 1978, 1981; Gage et al., 1980; Gossard et al., 1982; Doviak and Zrnić, 1984; Warnock and Van Zandt, 1985).

Rewriting (12) in terms of the vertical velocity component, $w$, we find it to be of the same form as (1). That is, under stable conditions ($\omega_B > 0$),

$$\frac{C_\theta^2}{C_W^2} = \frac{B_\theta}{B_W} \frac{\mathrm{Ri}}{\mathrm{Pr} - \mathrm{Ri}} \frac{\theta_0}{g} \frac{\partial \theta_0}{\partial z} = C_1 \frac{\theta_0}{g} \frac{\partial \theta_0}{\partial z} \equiv \frac{C_1}{\omega_B^2} \left( \frac{\partial \theta_0}{\partial z} \right)^2 . \tag{13a}$$

A similar derivation for humidity gives (Gossard and Sengupta, 1988)

$$\frac{C_Q^2}{C_W^2} = \frac{C_1}{C_r^2 \omega_B^2} \left( \frac{\partial Q}{\partial z} \right)^2 , \tag{13b}$$

where $C_r^2$ is the cross correlation (virtually unity in stable conditions) between temperature and humidity (see Fig. 6). Therefore,

$$\frac{C_\theta^2}{C_Q^2} = \frac{(\partial \theta_0 / \partial z)^2}{(\partial Q_0 / \partial z)^2} . \tag{13c}$$

When the spectra of $\theta$ and $w$ have the same functional form (e.g., proportional to $k^{-5/3}$) over all wavenumbers, then $C_\theta^2/C_V^2 = <\theta^2>/<w^2>$, where $\theta$ and $w$ are the perturbation components of potential temperature and vertical velocity.

## 3. RELATIONSHIP BETWEEN THE TURBULENT PRANDTL NUMBER AND THE RICHARDSON NUMBER

We note that the left side of (11) has dimensions of length raised to the 4/3 power (say $L_\theta^{4/3}$), as does the factor in square brackets at the right (say $L_V^{4/3}$) (Tatarskii, 1971), so (11) gives

$$\left(\frac{L_\theta}{L_V}\right)^{4/3} = \frac{B_\theta}{B}\,(\mathrm{Pr}-\mathrm{Ri})^{-1}\,. \tag{14}$$

Clearly, the length scales $L_\theta$ and $L_V$ will depend on stability and shear as expressed by Ri, and will be reduced under statically stable conditions because the work done against buoyancy will tend to flatten the eddy structure in the vertical direction.

Although $L_\theta$ and $L_V$ will not in general be equal, it is plausible that they will both be affected in a similar way by stability because the same eddy ensemble is responsible for the mixing of heat and momentum. Therefore, it is reasonable to suggest the hypothesis that $(L_\theta/L_V)^{4/3}$ is nearly constant, and it was proposed by Gossard et al. (1982) that (14) provides a unique relationship between Prandtl number and the Richardson number under the fully developed turbulent conditions described by (13).

The relationship between the turbulent Prandtl number and the Richardson number has periodically received considerable attention. The results of the different investigators are referenced by Kondo et al. (1978) and summarized in Fig. 1 (adapted from their Fig. 3). Our Eq. (14), which assumes steady, homogeneous conditions, is shown as the heavy solid line. It assumes that $K_V = K_\theta$ when Ri = 0 (a common assumption, but one with no solid basis from either experiment or theory).

Measurements by Gossard et al. (1984) lend support to the hypothesis that $L_\theta/L_V$ is approximately independent of stability. Data recorded on a 300-m meteorological tower (Kaimal and Gaynor, 1983) are shown in Figs. 2-4, and were compared with the relationships

$$\frac{C_\theta^2}{C_Q^2}\,\frac{(dQ_0/dz)^2}{(d\theta_0/dz)^2} \equiv \left(\frac{L_\theta}{L_Q}\right)^{4/3}, \quad \frac{C_\theta^2}{C_W^2}\,\frac{(dV_M/dz)^2}{(d\theta_0/dz)^2} \equiv \left(\frac{L_\theta}{L_W}\right)^{4/3} = \frac{B_\theta}{B_W}\,(\mathrm{Pr}-\mathrm{Ri})^{-1}\,, \tag{15}$$

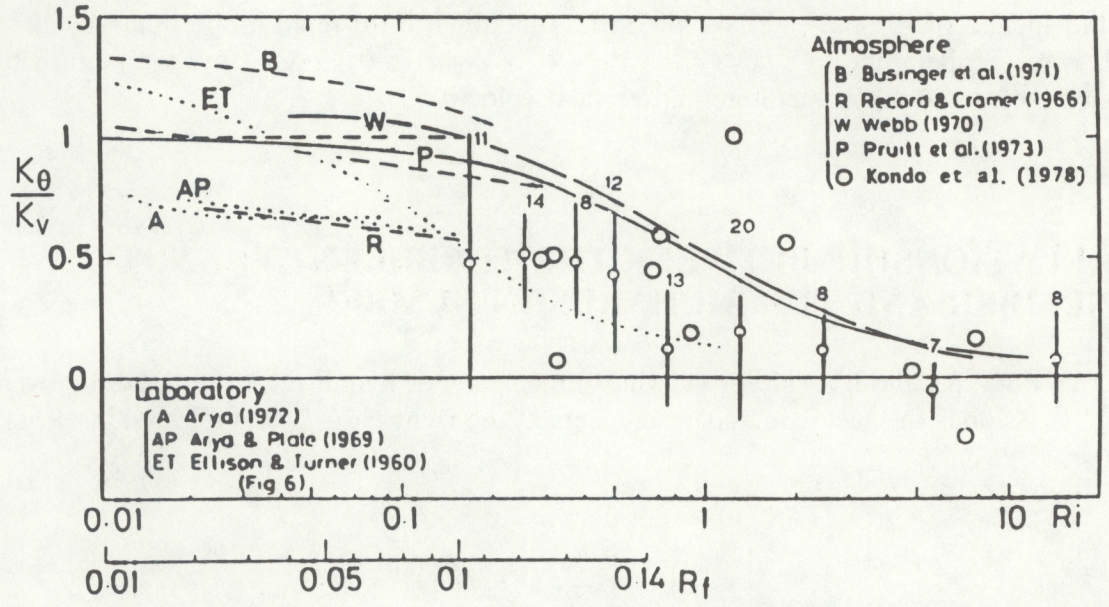


Fig. 1. Compilation of data from many workers, by Kondo et al. (1978), showing the relationship between the inverse turbulent Prandtl number $K_\theta/K_V$ and the Richardson number Ri. The small and large circles indicate 2-min and 30-min runs, respectively, by Kondo et al. The light short-dashed lines are other field results, and the dotted lines are laboratory results. The heavy solid and heavy long-dashed lines are theoretical results from the present paper. For references to specific data sets, see Kondo et al. (1978).

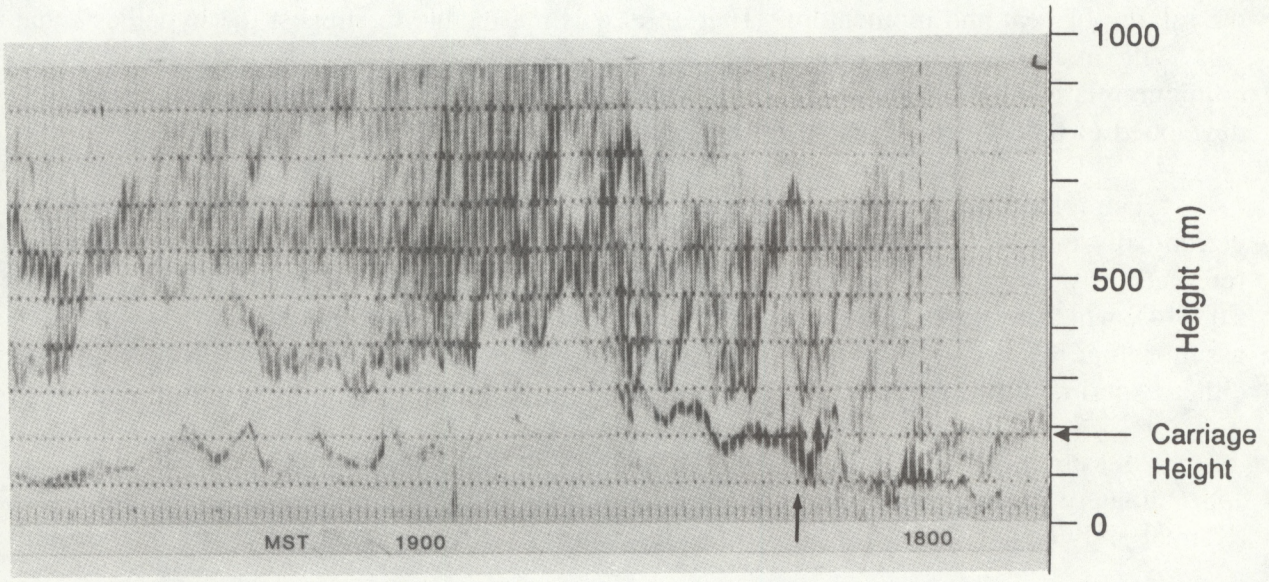


Fig. 2. Record from an FM-CW radar (Chadwick et al., 1976) situated about 300 m from the Boulder Atmospheric Observatory 300-m tower near Erie, Colorado. The record is from 10 February 1982 and alternately presents Doppler vertical velocity (quasi-horizontal dotted lines) and reflectivity, versus time and height. For this paper we analyzed data associated with the low layer of high reflectivity ascending from a height of about 100 m at 1800 MST to about 300 m at about 1840 MST. The arrow indicates the time of the sounding shown in Fig. 10.

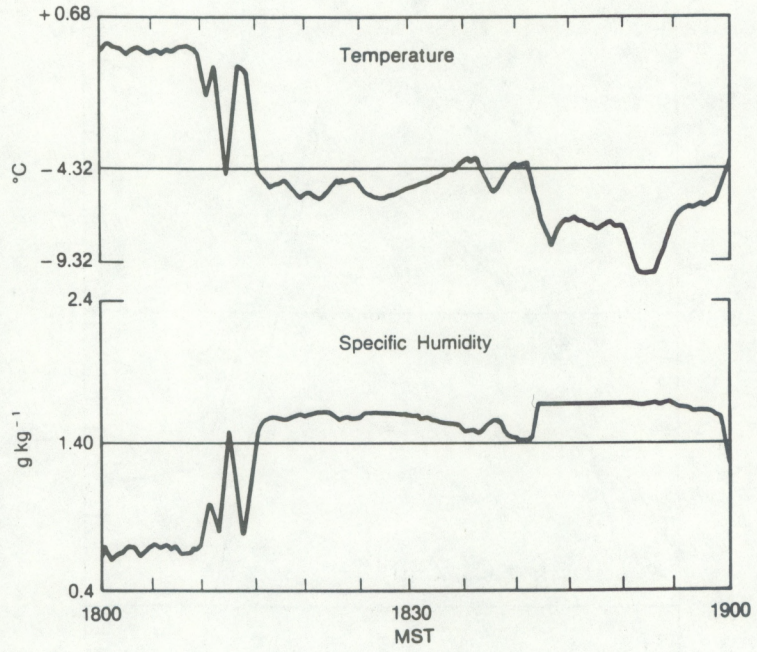


Fig. 3. Time series of temperature and humidity recorded by fast-response sensors on a boom from a carriage parked at the 175-m level of the 300-m BAO tower. This recording was made as the layer shown in Fig. 2 rose past the sensors on 10 February 1982.

where $Q$ is specific humidity. The ratios of length scales were found by measuring $C_\theta^2$, $C_Q^2$, and $C_W^2$ with platinum wire, Lyman-$\alpha$, and sonic anemometer sensors, and the means of the corresponding gradients were measured with slow-response (but more accurate) sensors. The results are presented in Fig. 5 as the product of measured $d\theta_0/dz$ and the appropriate ratio of length scales defined in (15). From (15) this product also shows the progression of $(B_\theta/B_W)(\mathrm{Pr} - \mathrm{Ri})^{-1}$ as the gradient layer studied in this paper rose past the sensors at the 175-m level. We note that the length scales of temperature and humidity were identical (on this plotting scale) until the direction of wind flow to the sensors passed through the tower structure after 1815 MST. However, the velocity scale was substantially smaller.

## 4. DESCRIPTION OF THE EXPERIMENTAL EVALUATION

Our ultimate goal is to deduce height gradients of humidity and radio refractive index from measurements made by surface-based, high-resolution clear-air radars (e.g., Richter, 1969; Ottersten, 1969; Atlas et al., 1970).

In the present case study, a vertically-pointing, 10-cm-wavelength, FM-CW radar (Chadwick et al., 1976) was located about 300 m from the meteorological tower near Erie, Colorado, operated by the Boulder Atmospheric Observatory (BAO) (Kaimal and Gaynor, 1983). In the climatic regime of Boulder, strong elevated layers occur only rarely below tower heights where measurements of the kind described above can be made. On 10 February 1982, the radar recorded a relatively strong layer as it traversed the tower. The

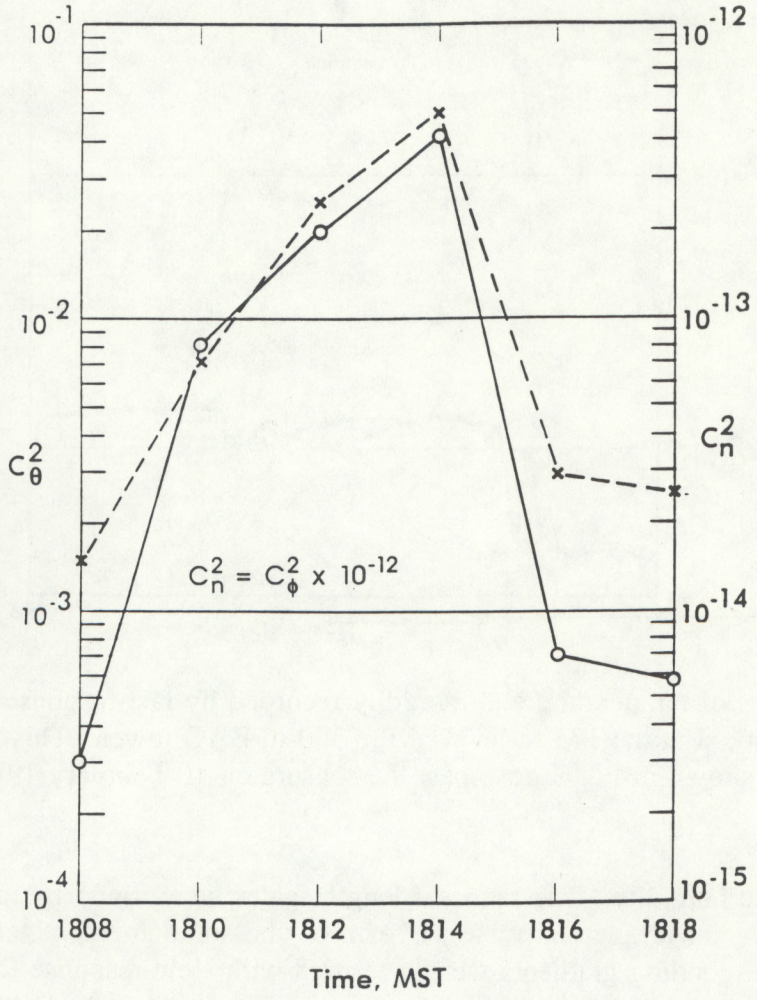


Fig. 4. The time history of temperature ($C_\theta^2$, dashed) and radio refractive index ($C_n^2 = C_\phi^2 \times 10^{-12}$, solid) structure parameters at the 175-m level of the tower as the layer shown in Fig. 2 ascended past the carriage sensors on 10 February 1982. $C_\phi^2$ was calculated from $C_\theta^2$ and $C_Q^2$ using (17), which is also readily used to calculate $C_Q^2$ when $C_\phi^2$ is given.

radar was pointing vertically, and it cycled automatically between the Doppler mode and the backscattered-power-vs.-range mode every minute, i.e., 15 s in Doppler and 45 s in range-power (see Fig. 2). Furthermore, at the time of this event the carriage was instrumented with the Lyman-α sensor and was at the 175-m level. This coincidence is rare; the Lyman-α humidometer is mounted only on special occasions because it must be recalibrated frequently due to drift. Also, the raw 10-Hz data were being recorded at that time, and so the spectra extended up to a frequency of 5 Hz (the Nyquist frequency). By contrast, the usual mode of operation archives data only at a sampling rate of one every 10 s. For all these reasons, this rare data set was analyzed intensively.

The time series of temperature and humidity are shown in Fig. 3, recorded with platinum wire and Lyman-α sensors, as the layer traversed the 175-m level of the 300-m tower. From these data the refractivity (Bean and Dutton, 1966) was calculated from

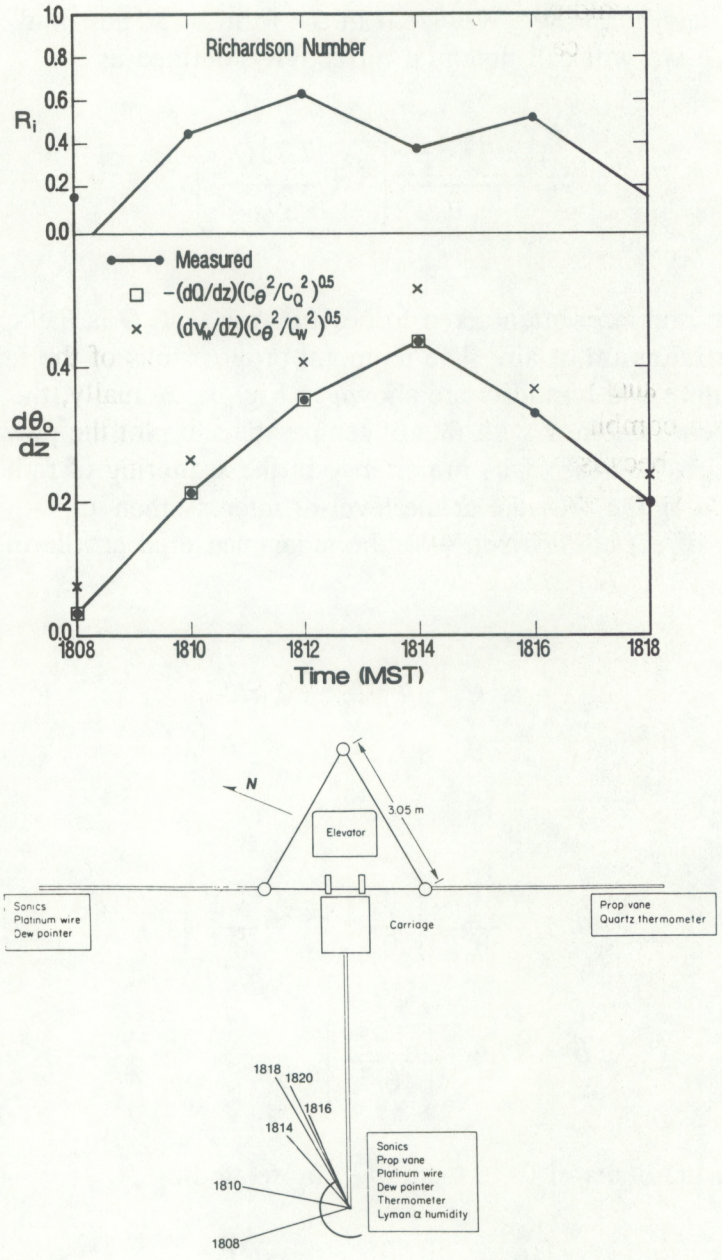


Fig. 5. Top frame: Averaged values of Ri calculated from sensors at the 150- and 200-m levels, 10 February 1982. Middle frame: The product of the measured temperature gradient $d\theta_0/dz$ and the ratio to the two-thirds power of the length scale for temperature to the length scales for temperature $L_\theta$ and humidity $L_Q$ deduced from $C_\theta^2$ and $C_Q^2$, respectively, and to a length scale $L_W$ calculated from the measured wind shear and $C_W^2$. Bottom frame: Tower boom configuration showing the exposure of sensors located on the boom ends. Note that the carriage sensors (bottom) are contaminated by tower-generated turbulence after 1815 MST, as shown by the wind direction change indicated by the orientation of the time-labeled radial lines centered near the carriage. Until 1815 MST, the agreement of the measured $d\theta_0/dz$ and that calculated from the humidity gradient is extremely good ($L_\theta/L = 1$), but the corresponding calculated value based on the wind gradient (i.e., $L_\theta/L_W < 1$) lies well above the measured value, and provides an indirect measure of the turbulent Prandtl number [see Eq. (15)].

pressure, temperature, and humidity. We use it in the form of a "potential" radio refractive index times $10^{12}$, which we will call potential refractivity, defined as

$$\phi_0 = \frac{77.6\,p_r}{\theta_0}\left(1 + \frac{7.73\,Q_0}{\theta_0}\right), \tag{16}$$

where $p_r$ is a reference pressure, often taken to be 1000 mb, and $Q$ is the specific humidity in grams of moisture per kilogram of air. The temporal progressions of the turbulent structure parameters of temperature and humidity are shown in Fig. 4. Actually, the structure parameter of humidity has been combined with that of temperature to plot the potential refractivity structure parameter, $C_\phi^{\,2}$, because of its importance in the scattering of radiowaves in the clear atmosphere. (If $p_r$ is the pressure at the level of interest, then $C_n^{\,2} = C_\phi^{\,2} \times 10^{-12}$, which is plotted in Fig. 4 for direct comparison with the radar-measured profile of $C_n^{\,2}$ in Fig. 10.) It is given by

$$C_\phi^{\,2} = a^2 C_\theta^{\,2} + b^2 C_Q^{\,2} - 2\,ab\,C_{\theta Q}^{\,2}\,, \tag{17}$$

where

$$a = \frac{77.6\,p_r}{\theta_0}\left(\frac{1}{\theta_0} + 15.46\,\frac{Q_0}{\theta_0^{\,2}}\right),$$

$$b = 77.6\,p_r\left(\frac{7.73}{\theta_0^{\,2}}\right),$$

and the corresponding gradients of $\phi$ , $\theta$ , and $Q$ are related by

$$\frac{\partial \phi_0}{\partial z} = -a\,\frac{\partial \theta_0}{\partial z} + b\,\frac{\partial Q_0}{\partial z}\,. \tag{18}$$

The time series of $C_\phi^{\,2}$ and $C_Q^{\,2}$ were used to test the relationships in (15). When the temperature and humidity fluctuations are perfectly (negatively) correlated [which is almost true under stable conditions (Gossard et al., 1984) such as this case as shown in Fig. 6], we note that $C_{\theta Q}^{\,2} = -C_\theta\,C_Q$ .

To compare theory with measurements, we plotted the product of the ratios of the length scale for temperature to the various length scales for temperature, humidity, and vertical velocity [all found from (15)] and the measured temperature gradient. If the length scales are the same, the product is simply the measured temperature gradient. If they are not,

they provide measures of quantities such as turbulent Prandtl number. The results are shown in Fig. 5. A wind shift accompanied the event, as shown by the radial line segments representing wind direction in the bottom frame, and the wind swung into a northeasterly direction that brought tower-generated mechanical turbulence to the carriage instruments after 1815 MST. Therefore, we attempted to use turbulence quantities from the 150-m and 200-m levels (platinum wire and sonics only) after 1814 MST, and the averaged values for these levels are shown for 1816 and 1818 MST in Fig. 5. In Fig. 5 the agreement in the ordinate value deduced from the turbulent temperature and humidity structure parameters is quite remarkable

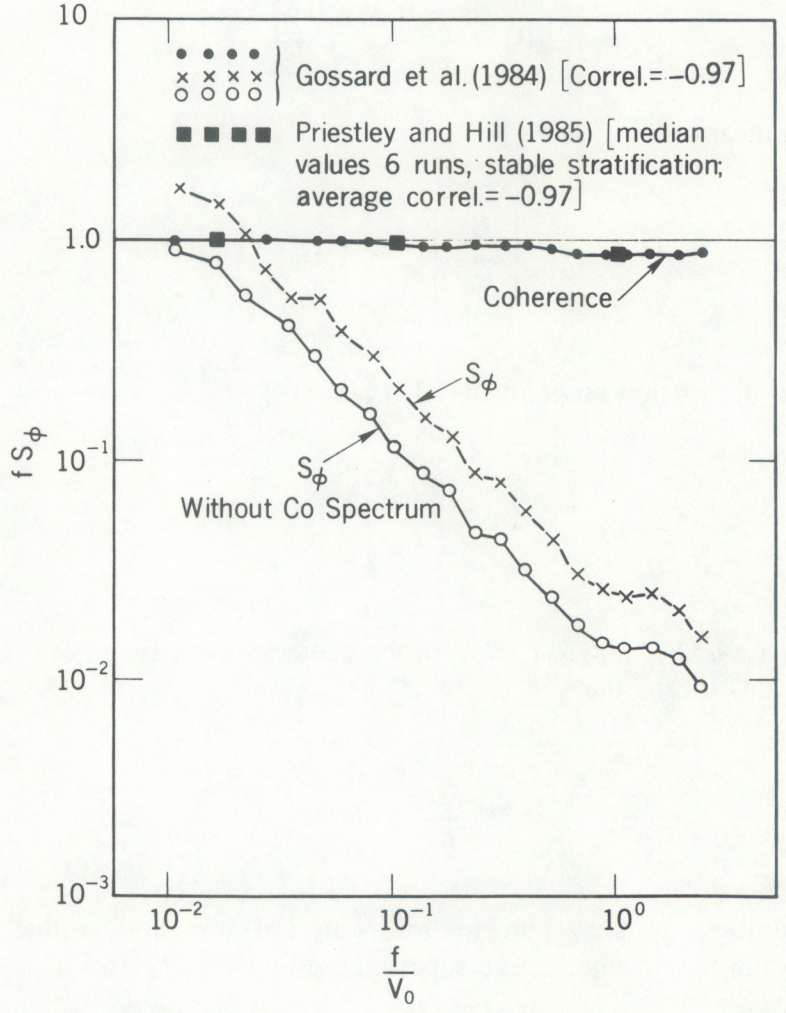


Fig. 6. Spectra of potential radio refractivity, $S_\phi$, within the stable elevated layer of 10 February 1982, described in Figs. 2-5. The potential refractivity was calculated from (16) using Lyman-$\alpha$ measurements of humidity and platinum wire measurements of temperature. $S_\phi$ calculated with (crosses) and without (open circles) the cospectral contribution are shown. The contribution of the cospectrum is large because of the very high correlation (-0.97) between temperature and humidity; in fact, the temperature-humidity coherence (filled circles) is about 0.8 down to the smallest scales measurable in the experiment. Similar high correlation (-0.97) and coherence (filled squares) of temperature and humidity measured in the stable surface layer by Priestley and Hill (1985) are shown.

before 1815 MST when the carriage-measured values were used; therefore these data strongly suggest $L_Q \simeq L_\theta$ . After 1815 MST, when the averaged fixed-level values of $C_\theta^2$ from 150 and 200 m were used, the same trends are evident, but because there were no Lyman-$\alpha$ humidity measurements at these levels, $L_Q$ is missing. The products of temperature gradient and length scale found from the wind field lie substantially above both the measured temperature gradients and those deduced from $C_Q^2$. Using the three carriage values within the ascending layer at 1810, 1812, and 1814 MST, we see that the adjustment needed to bring the wind field values into agreement with the others would require [see (15)]

$$\frac{B_W}{B_\theta}(\mathrm{Pr} - \mathrm{Ri}) \simeq 0.67 ,$$

and from (14) this means that

$$\left(\frac{L_\theta}{L_W}\right)^{4/3} \simeq 1.33 .$$

So, in the turbulent dissipation range, using (13) and (14),

$$C_1 = \left(\frac{L_\theta}{L_W}\right)^{4/3} \mathrm{Ri} . \qquad (19)$$

If the values of $B_W (=4/3B)$ and $B_\theta (=B_\phi)$ in the center of their range of estimate (shown in Table 1) are used, this means that

$$\frac{K_V}{K_\theta} \simeq 0.86$$

under neutral conditions. If the arguments following (14) are valid, so that $L_\theta/L_V \simeq$ constant, this leads to the long-dashed curve superimposed on Fig. 1. In Fig. 7, $C_1$ is shown plotted from (13).

The following points should be noted:

(1) The equality of $L_\theta$ and $L_Q$ is supported by the data presented here.

(2) The data presented here lead to a value of $(L_\theta/L_W)^{4/3} \simeq 1.33$ (or $L_\theta/L_W \cong 1.24$) and a turbulent Prandtl number of 1.36 for the Ri associated with these data. This suggests that $C_1 \simeq 1.33$ Ri within the inertial subrange of turbulence.

Table 1. Turbulence parameters

| Relationships | Range of values |
|---|---|
| *Velocity Field* | |
| $E(k) = \alpha \varepsilon^{2/3} k^{-5/3}$ | $\alpha = 1.53-1.68$ |
| $S(k_1) = A \varepsilon^{2/3} k_1^{-5/3}$ | $A = 0.50-0.55$ |
| $D_u(l) = \overline{[u(x+l) - u(x)]^2} = \underbrace{B \varepsilon^{2/3}}_{C_V^2} l^{2/3}$ | $B = 2.0-2.2$ |
| *Potential Refractivity Field (and Other Passive Scalar Fields)* | |
| $E_\phi(k) = \alpha_\phi \varepsilon^{-1/3} \varepsilon_\phi k^{-5/3}$ | $\alpha_\phi = 1.33-1.67$ |
| $S_\phi(k_1) = A_\phi \varepsilon^{-1/3} \varepsilon_\phi k_1^{-5/3}$ | $A_\phi = 0.8-1.0$ |
| $D_\phi(l) = \underbrace{B_\phi \varepsilon^{-1/3} \varepsilon_\phi}_{C_\phi^2} l^{2/3}$ | $B_\phi = 3.2-4.0$ |

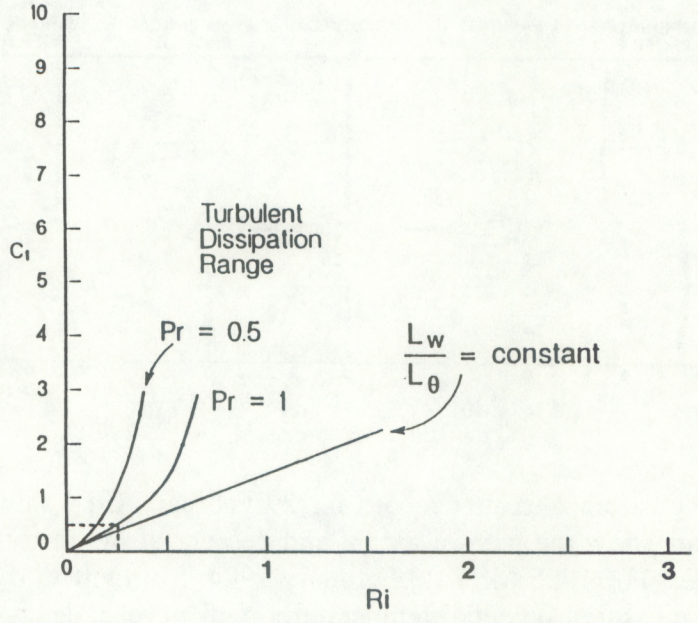


Fig. 7. The factor $C_1$ versus Ri from (13) over the range of turbulent production-dissipation equilibrium. Curves are calculated from (13) assuming Pr = 0.5 and Pr = 1.0, and from (13) and (15) assuming $L_\theta/L_W$ is independent of Ri.

To test further the relationships between variance and gradient in (13), we used observational data from Gossard et al. (1985) for 29 February 1984, shown here in Fig. 8. The top frame shows the time-height distribution of acoustic backscatter from a stable, laminated boundary layer near the BAO tower. The line segments show the path of the carriage through the multiple layered structure. The bottom frame shows the tower-carriage-measured mean temperature profile, the corresponding height profile of potential temperature gradient, the retrieved potential temperature gradient, and the height profiles of inverse $w$-variance and temperature variance. The center profile of the height distribution of the potential temperature gradient was calculated from (13) assuming $C_1 = 1$. The profile at 1055 MST was chosen for illustration because only a single, well-defined layer was present

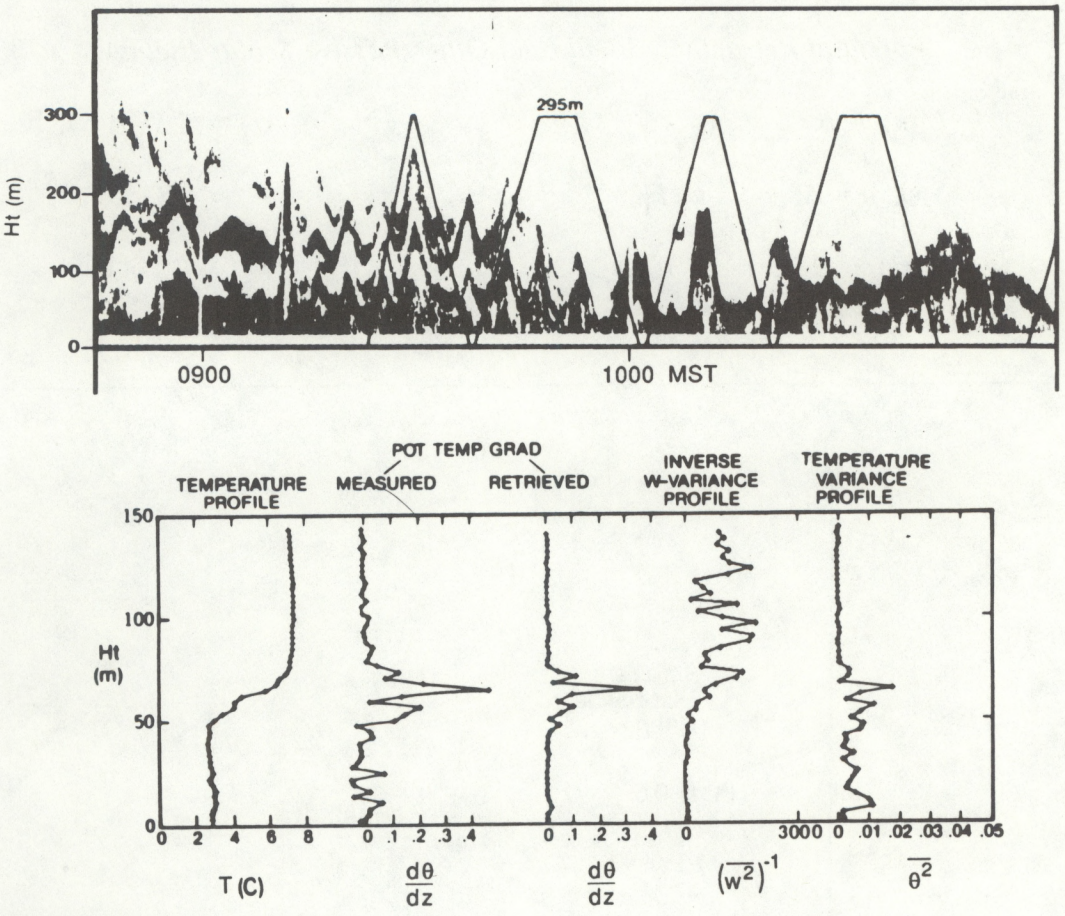


Fig. 8. Top frame: Acoustic backscatter record for 29 February 1984 showing layer fine structure. Line segments show the path of ascent and descent of the instrumented tower carriage. Bottom frame: For 1055 MST 29 February 1984, from left to right, profiles of measured temperature, measured potential temperature gradient, calculated potential temperature gradient, i.e., the product of inverse variance of $w$ and variance of temperature, assuming $C_1 = 1.0$; inverse variance of $w$; and variance of temperature. This carriage run was chosen because only a single, well-defined layer was present.

in that profile. The results were similar for the other passes, but were often very complex. For example, the carriage ascent beginning at 1002 MST passed through the same layer twice because, for a time, the layer rose more rapidly than the sensor as a result of a wave perturbation, and thus falsely indicated two layers.

## 5. REMOTE MEASUREMENT OF HUMIDITY AND REFRACTIVE INDEX GRADIENTS

The general result corresponding to (13) is (Gossard and Sengupta, 1988)

$$\frac{C_\chi^{\,2}}{C_W^{\,2}} = \frac{C_1}{\omega_B^{\,2}} \left( \frac{\partial \chi_0}{\partial z} \right)^2 C_r^{\,-2} , \tag{20}$$

where $\chi$ can be any passive scalar having the same spectral form as $w$. The absolute value of the correlation, $C_r$, between temperature and humidity (and therefore between $\theta$ and $\phi$) has been shown to be very nearly unity even down to small scales (coherence $\approx$ 1 out to high frequencies) under statically stable conditions (Gossard, 1960; Gossard et al., 1984; Priestley and Hill, 1985). (See, e.g., Fig. 6.)

Experimental justification for extending the result for temperature (13) to humidity $Q$ and refractive index $\phi$ (20) is shown in Fig. 9.

The following points should be emphasized:

(1) Radars can remotely measure $C_n^{\,2}$ (and therefore $C_\phi^{\,2}$) to high accuracy in the absence of clouds or other particulates (e.g., compare Figs. 4 and 10). Doppler radars can also (in principle) measure $C_W^{\,2}$ from the turbulent broadening of the Doppler spectrum (Frisch and Clifford, 1974; Gossard et al., 1990). Such radars, with a Radio Acoustic Sounding System (RASS), can also measure both temperature and wind profiles, and therefore can provide $\omega_B^{\,2}$ and Ri. Thus, from radar data, $\partial \phi_0 / \partial z$ can be calculated, and, from (18), $\partial Q_0 / \partial z$ can then be found. In practice, the measurement of the spectral width is difficult because of spectral broadening by effects other than turbulence, such as substantial antenna beamwidth in the presence of transverse winds, and wind shear. Furthermore, accurate second moments require high signal-to-noise ratios.

(2) A more direct approach that bypasses the second-moment calculation and also the need for assuming, or deducing, $C_1$, makes use of a direct measurement of $C_\theta^{\,2}$ from the acoustic backscatter from the RASS transmission, since the acoustic $C_n^{\,2}$ depends almost exclusively on $C_\theta^{\,2}$. The modulation schemes used in the present generation of experimental RASS systems preclude use of the acoustic backscatter from RASS, so a separate acoustic sounder will initially be needed to evaluate the concept. From (13c), (15), (17), and (18),

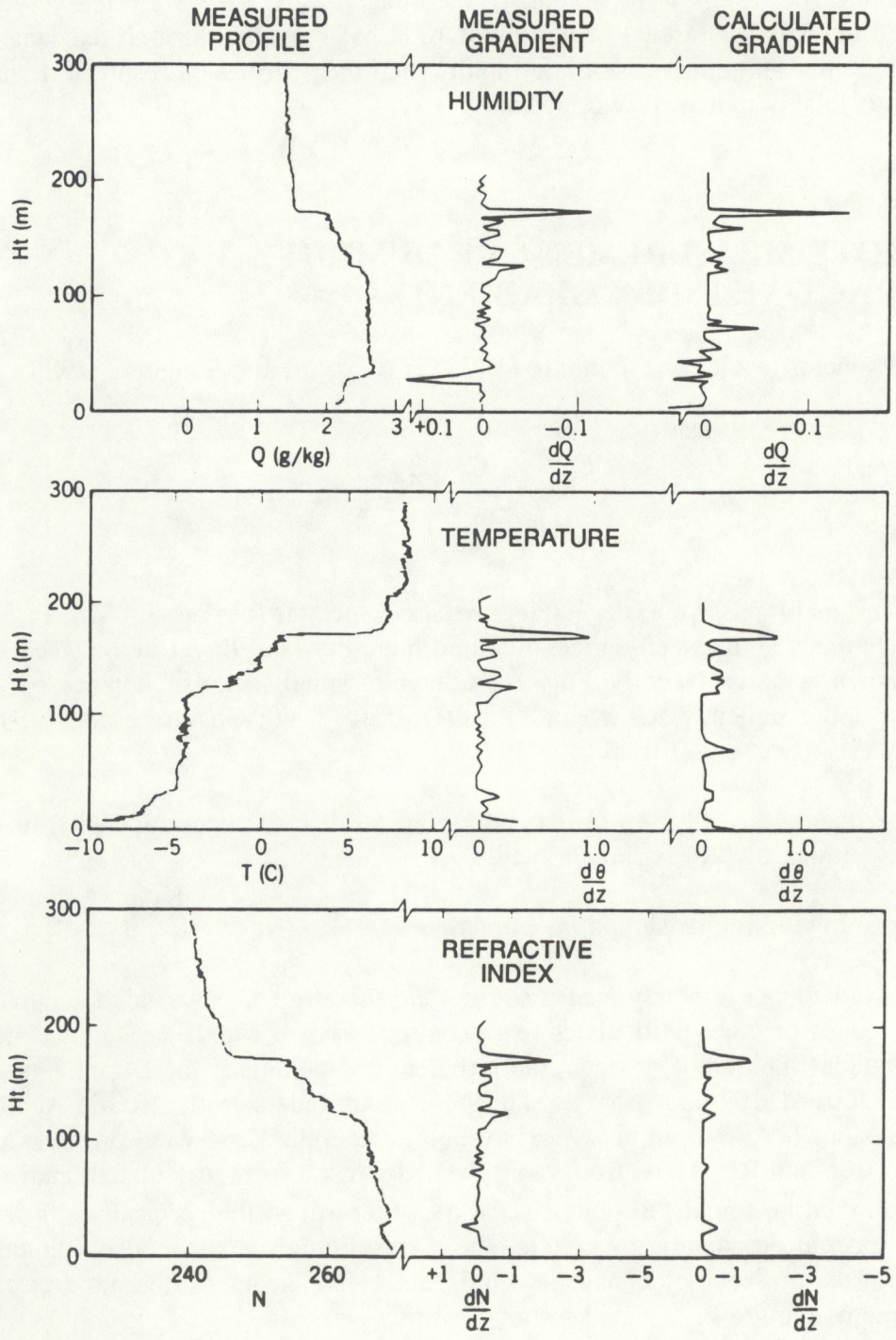


Fig. 9. Left profiles: Mean values of humidity (top), temperature (middle), and radio refractive index (bottom). Middle profiles: Measured gradients. Right profiles: Gradients calculated from variances of humidity, temperature, and vertical velocity using (20), assuming $C_1 = 1.0$ and $C_r = -1$. The measured gradients (middle) were found from profiles of the mean quantities (left). Data were obtained on 29 December 1985 at 0523 MST, with Lyman-α, platinum wire, and sonic anemometer sensors on a carriage traversing the BAO tower (Gossard and Sengupta, 1988). $N = (77.6\,p/T)\,[1 + (7.73\,Q/T)]$, where $T$ is temperature (K), $p$ is pressure (mb), and $Q$ is specific humidity (g kg$^{-1}$) (Bean and Dutton, 1966).

$$\left(\frac{\partial \phi_0}{\partial z}\right)^2 = \frac{C_\phi^{\,2}}{C_\theta^{\,2}}\left(\frac{\partial \theta_0}{\partial z}\right)^2 . \tag{21}$$

With $C_\phi^{\,2}$ and $\partial\theta_0/\partial z$ available from a radar with RASS, and $C_\theta^{\,2}$ available (in principle) from the acoustic backscatter, $|\partial\phi_\theta/\partial z|$ can immediately be calculated. The sign ambiguity would seldom be a major problem because temperature inversions and super adiabatic gradients are well-understood features of most synoptic situations. From (18) we readily find the humidity gradient, i.e.,

$$\frac{\partial Q_0}{\partial z} = \frac{1}{b}\frac{\partial \phi_0}{\partial z} + \frac{a}{b}\frac{\partial \theta_0}{\partial z} , \tag{22}$$

and note that the value of $\theta_0$ needed in $a$ and $b$ is provided by RASS, and a first estimate of $Q_0$ is provided by microwave radiometers or local climatology.

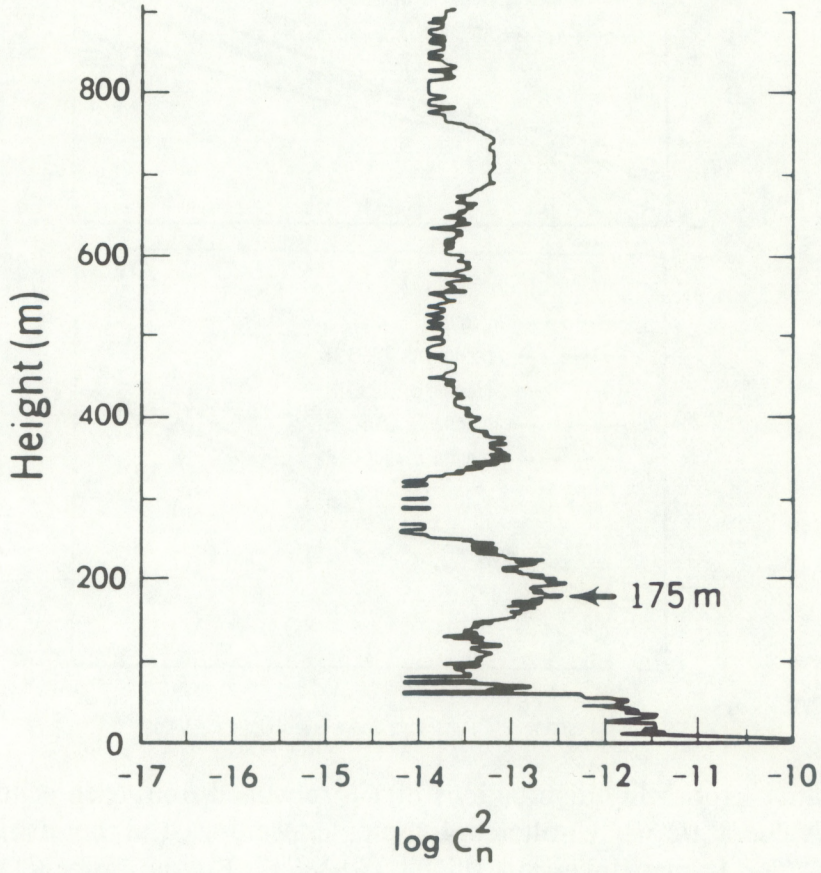


Fig. 10. Radar-measured profile of log $C_n^{\,2}$ (where $C_n^{\,2} = C_\phi^{\,2} \times 10^{-12}$ ) at 1814 MST on 10 February 1982 when a strongly refractive layer crossed the 175-m level on the tower. Compare this figure with Figs. 2 and 4 to note the excellent agreement of $C_n^{\,2}$ at 175 m with the $C_n^{\,2}$ value at 1814 MST in Fig. 4.

A variety of experimental results (e.g., Kropfli et al., 1968; Bean et al., 1971) support the ability of well-calibrated radars to measure $C_n^2$ (and therefore $C_\phi^2 = C_n^2 \times 10^{12}$) accurately in clear-air conditions. For the case study of 10 February 1982 discussed in this report, the reader should compare the profile of $C_n^2$ shown in Fig. 10, measured by radar, with the temporal record of radar backscatter shown in Fig. 2, and with the tower-measured Lyman-$\alpha$ and platinum wire measurements of $C_n^2 = C_\phi^2 \times 10^{-12}$ (calculated from the humidity and temperature components) shown in Fig. 4. The value of $C_n^2$ measured by the radar at 175 m at 1814 MST is in very reassuring agreement with the measurement at that time and height by the in situ sensors.

The ability of acoustic sounders to sense $C_\theta^2$ accurately is not so well established. The pioneering work was done by Neff (1975); see Fig. 11. Much of the recent experimental

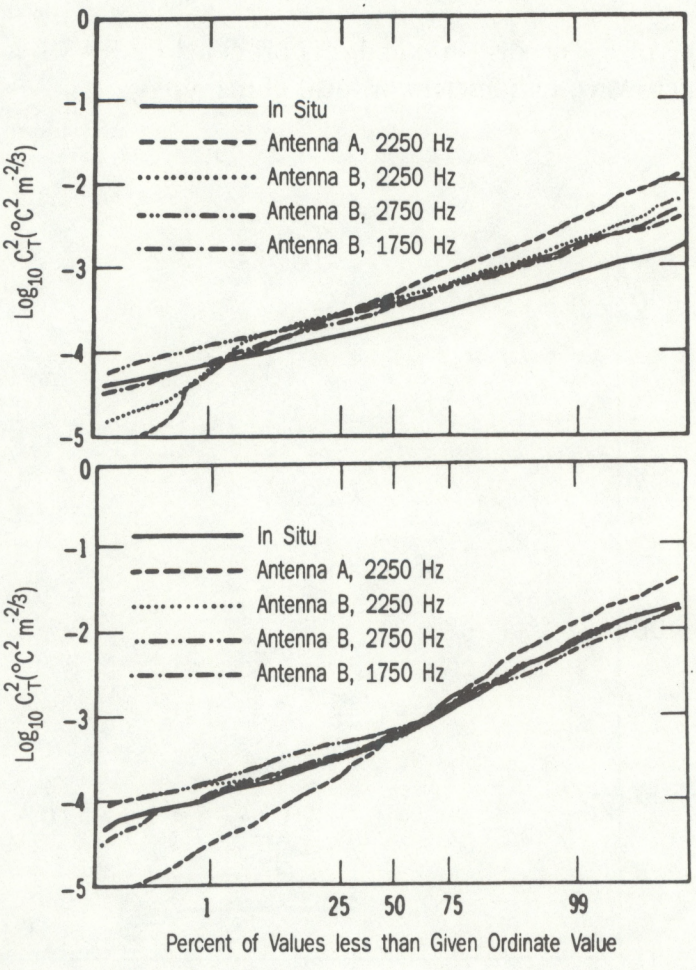


Fig. 11. Cumulative probability distributions of $C_T^2$ obtained from each echosonde and the tower-measured value at 92 m. Unfiltered 4-s samples were used in the distributions on 15 August 1972. Top frame: Inversion, 0510-0730 MST. Bottom frame: Developing convection, 0730-1000 MST. The plots show the percentage of values that are less than the given ordinate value (Neff, 1975). Antenna A was pointed vertically and used a frequency of 2250 Hz. Antenna B was pointed 30° off vertical, and transmitted at frequencies of 2250, 2750, and 1750 Hz.

work has been done by the Atmospheric Sciences Laboratory of White Sands Missile Range (e.g., Chintawongvanich and Olsen, 1991), and some recent comparisons reported by Eaton (1992) are shown in Fig. 12 where log $C_n^2$ is plotted versus time; data are from the sodar and from the tower-mounted $C_T^2$ sensor at heights of 23, 68.5, and 152 m. The agreement is obviously very good, but the author cautions that these are the best comparisons to date, and that the comparisons become erratic under stable conditions at night, probably because of

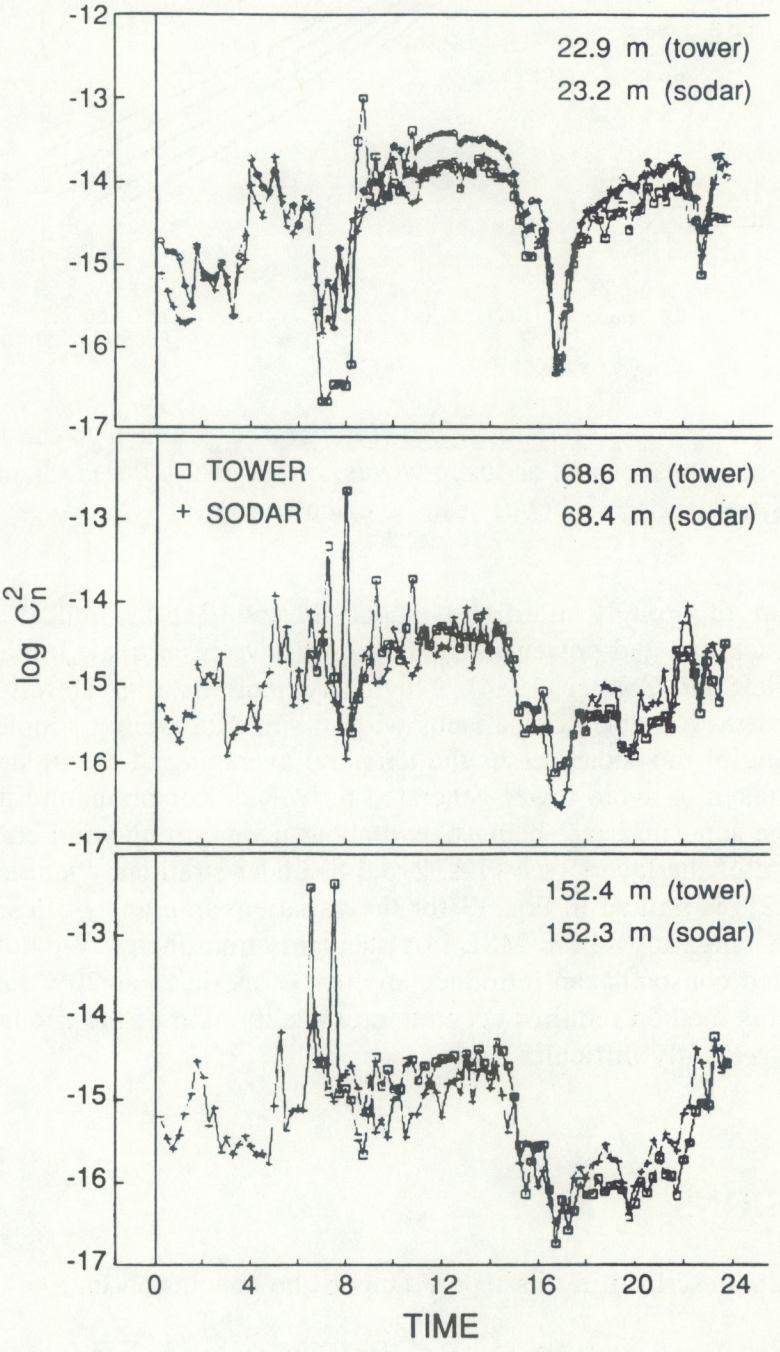


Fig. 12. Comparison of log $C_n^2$ measured acoustically (pluses), and measured by a tower-mounted $C_T^2$ sensor (open boxes), at White Sands, 23 October 1991. The acoustic and in situ values agree very well after 0930 MST (Eaton, 1992).

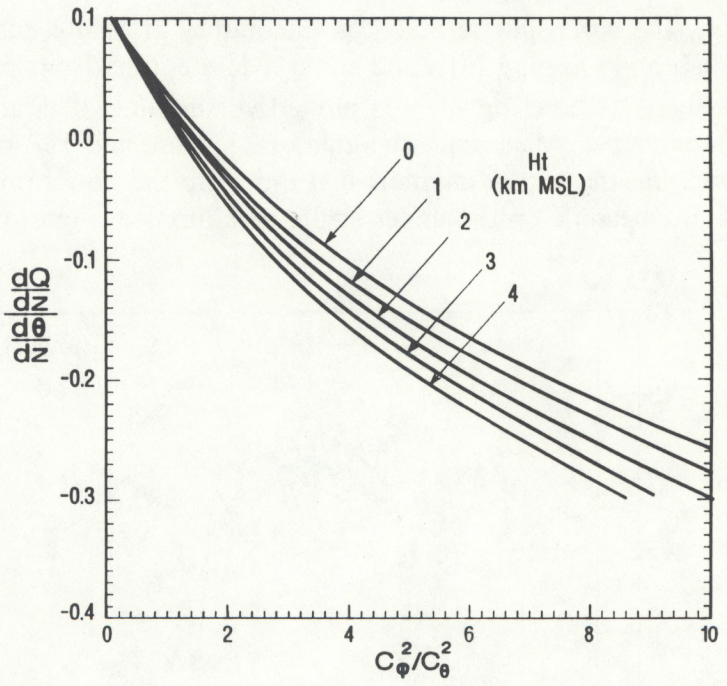


Fig. 13. Plot of $C_\phi^2/C_\theta^2$ vs. the ratio $(dQ/dz)/(d\theta/dz)$. $C_\phi^2$ and $C_\theta^2$ can be calculated from the backscatter of radar waves and acoustic waves, respectively; the gradient $d\theta/dz$ can be found from RASS (see text), so $dQ/dz$ can be calculated.

the laminated nature of strongly stratified boundary layers. The theoretical considerations relating acoustic backscattered power to $C_T^2$ ( = $C_\theta^2$) have been treated in a comprehensive review paper by Neff and Coulter (1984). Obviously, more data in carefully controlled conditions are needed. Suitable comparisons with in situ data are not simple because of (1) the spatial averaging of the sodar versus the temporal averaging of the in situ sensor, (2) the care that must be taken to avoid tower-generated turbulence contaminating the in situ sensor, (3) the effect of the acoustic beam being blown about under strong wind conditions, and (4) the very thin nature of the layers (see Figs. 2 and 8) under stratified conditions. The solution of Eqs. (20) and (21) is plotted in Fig. 13 for the variations in $a$ and $b$ [Eqs. (17), (18), and (22)] over a height range of 0-4 km MSL in a standard atmosphere. We note that treating $a$ and $b$ as uncorrected constants can introduce an error of as much as 20% for $C_\phi^2/C_\theta^2 = 6$. We also see that this method requires accurate cross-calibration of the acoustic and radar systems, which is generally difficult.

## 6. CONCLUSIONS

(1) The data described in this report support the conclusion that

$$C_\theta^2(\partial\theta_0/\partial z)^{-2} = C_Q^2(\partial Q_0/\partial z)^{-2}.$$

(2) From these data we conclude that $C_\theta^2(\partial\theta_0/\partial z)^{-2} \approx 1.33\, C_W^2(\partial V_M/\partial z)^{-2}$ from which we find a turbulent Prandtl number of about 1.36 for the bulk Ri associated with these data. This suggests that the excitation factor $C_1 \approx 1.33$ Ri within the turbulent inertial range, and that $\mathrm{Pr} \approx 0.86$ under neutral stability conditions.

(3) Radars can remotely measure $C_\phi^2$ to high accuracy in the absence of clouds or other particulates. Doppler radars can also (in principle) measure $C_W^2$ from the turbulent broadening of the Doppler velocity spectrum. Such radars, used with a Radio Acoustic Sounding System (RASS), can also measure both temperature and wind profiles; therefore they can provide the Richardson number and the Väisälä-Brunt frequency. The refractive index gradient can then be calculated from (20) and the humidity gradient from (18).

(4) A more direct approach for measuring the humidity gradient $\partial Q_0/\partial z$ that would avoid $C_1$ and the necessity for the difficult measurement of spectral broadening, needed in the above method, makes use of the direct measurement of $C_\theta^2$ from the acoustic backscatter from the RASS system. If we measure $C_\theta^2$ from the acoustic backscattered power, $C_\phi^2$ from the radar backscatter, and $\partial\theta_0/\partial z$ from the RASS, then $\partial\phi_0/\partial z$ is available from (45) and $\partial Q_0/\partial z$ can be found from (22).

## 7. ACKNOWLEDGMENTS

This work was supported by the Naval Command, Control and Ocean Surveillance Center (Contract Monitor, J. H. Richter). The author also wishes to acknowledge important advice and consultation with F. Eaton, C. W. Fairall, A. S. Frisch, J. E. Gaynor, W. D. Neff, J. A. Schroeder, B. B. Stankov, R. G. Strauch, and D. E. Wolfe.

## 8. REFERENCES

Atlas, D., J.I. Metcalf, J.H. Richter, and E.E. Gossard, 1970: The birth of "CAT" and microscale turbulence. *J. Atmos. Sci., 27*, 903-913.

Bean, B.R., and E.J. Dutton, 1966: *Radio Meteorology*. NBS Monograph 92, National Bureau of Standards, Boulder, CO, 435 pp.

Bean, B.R., R.E. McGavin, R.B. Chadwick, and B.B. Warner, 1971: Preliminary results of utilizing the high resolution FM radar as a boundary layer probe. *Bound.-Layer Meteor., 1*, 466-473.

Businger, J.A., 1982: Equations and concepts. In *Atmospheric Turbulence and Air Pollution Modeling*, F.T.M. Nieuwstadt and H. van Dop (eds.). Reidel, Dordrecht, 1-36.

Chadwick, R.B., K.P. Moran, R.G. Strauch, G.E. Morrison, and W.C. Campbell, 1976: A new radar for measuring winds. *Bull. Amer. Meteor. Soc., 57*, 1120-1125.

Chintawongvanich, P., and R. Olsen, 1991: Experimental study of temperature structure parameter in the surface layer. Proceedings, 7th Symposium on Meteorological Instrumentation, New Orleans, LA, January 1991. American Meteorological Society, Boston, 413-418.

Corrsin, S., 1951: On the presence of isotropic temperature fluctuations in an isotropic turbulence. *J. Appl. Phys., 22*, 417-423.

Doviak, R.J., and D.S. Zrnic, 1984: *Doppler Radar and Weather Observations.* Academic Press, London, 458 pp.

Eaton, F., 1992: HIDL site. SLCAS-BW-R, Atmospheric Sciences Laboratory, White Sands Missile Range, NM, 28 pp.

Frisch, A.S., and S.F. Clifford, 1974: A study of convection capped by a stable layer using Doppler radar and acoustic echo sounders. *J. Atmos. Sci., 31*, 1622-1628.

Gage, K.S., J.L. Green, and T.E. Van Zandt, 1980: Use of Doppler radar for the observations of atmospheric turbulence parameters from the intensity of clean air echoes. *Radio Sci., 15*, 407-416.

Gossard, E.E., 1960: Power spectra of temperature, humidity, and refractive index from aircraft and tethered balloon measurements. *IEEE Trans. Antennas Propag., AP-8*, 186-201.

Gossard, E.E., and N. Sengupta, 1988: Measuring gradients of meteorological properties in elevated layers with a surface-based Doppler radar. *Radio Sci., 23*, 625-693.

Gossard, E.E., R.B. Chadwick, W.D. Neff, and K.P. Moran, 1982: The use of ground-based Doppler radars to measure gradients, fluxes and structure parameters in elevated layers. *J. Appl. Meteor., 21*, 211-226.

Gossard, E.E., R.B. Chadwick, T.R. Detman, and J.E. Gaynor, 1984: Capability of surface-based, clear-air Doppler radar for monitoring meteorological structure of elevated layers. *J. Clim. Appl. Meteor., 23*, 474-490.

Gossard, E.E., J.E. Gaynor, R.J. Zamora, and W.D. Neff, 1985: Fine structure of elevated stable layers observed by sounder and in situ tower sensors. *J. Atmos. Sci., 42*, 2156-2169.

Gossard, E.E., D.C. Welsh, and R.G. Strauch, 1990: Radar-measured height profiles of $C_n^2$ and turbulence dissipation rate compared with radiosonde data during October 1989 at Denver. NOAA Technical Report ERL 442-WPL 63, NOAA Environmental Research Laboratories, Boulder, CO, 115 pp.

Kaimal, J.E., and J.E. Gaynor, 1983: The Boulder Atmospheric Observatory. *J. Appl. Meteor., 22*, 863-880.

Kondo, J., O. Kanechika, and N. Yasuda, 1978: Heat and momentum transfers under strong stability in the atmospheric surface layer. *J. Atmos. Sci., 35*, 1012-1021.

Kropfli, R. A., I. Katz, T. G. Konrad, and E. B. Dobson, 1968: Simultaneous radar reflectivity measurements and refractive index spectra in the clear atmosphere. *Radio Sci., 3*, 991-994.

Lumley, J.L., and H.A. Panofsky, 1964: *The Structure of Atmospheric Turbulence.* Wiley, New York, 239 pp.

Neff, W.D., 1975: Quantitative evaluation of acoustic echoes from the planetary boundary layer. NOAA Technical Report ERL 322-WPL 38, NOAA Environmental Research Laboratories, Boulder, CO, 34 pp.

Neff, W.D., and R.L. Coulter, 1984: Acoustic remote sensing. In *Probing the Atmospheric Boundary Layer*, D. Lenschow (ed.). American Meteorological Society, Boston, 201-241.

Ottersten, H., 1969: Atmospheric structure and radar backscattering in clear air. *Radio Sci., 4*, 1179-1193.

Priestley, J.T., and R.J. Hill, 1985: Measuring high-frequency humidity, temperature, and radio refractive index in the surface layer. *J. Atmos. Oceanic Technol., 2*, 233-251.

Richter, J.H., 1969: High-resolution tropospheric radar sounding. *Radio Sci., 4*, 1260-1268.

Tatarskii, V.I., 1971: *The Effects of the Turbulent Atmosphere on Wave Propagation.* U.S. Department of Commerce, National Technical Information Service, Springfield, VA (N72-18163), 472 pp.

Van Zandt, T.E., J.L. Green, K.S. Gage, and W.L. Clark, 1978: Vertical profiles of refractivity turbulence structure constant: Comparison of observations by the Sunset radar with a new theoretical mode. *Radio Sci., 13*, 819-829.

Van Zandt, T.E., K.S. Gage, and J.M. Warnock, 1981: An improved model for the calculation of profiles of $C_n^2$ and $\varepsilon$ in the free atmosphere from background profiles of wind, temperature, and humidity. Proceedings, 20th Conference on Radar Meteorology, Boston, MA, Nov. 30-Dec. 3, 1981. American Meteorological Society, Boston, 129-135.

Warnock, J.M., and T.E. Van Zandt, 1985: A statistical model to estimate the refractivity turbulence structure constant $C_n^2$ in the free atmosphere. NOAA Technical Memorandum ERL AL-10, NOAA Environmental Research Laboratories, Boulder, CO, 175 pp.

*U.S. GOVERNMENT PRINTING OFFICE: 1992-774-025/69040